Near-infrared-assisted charge control and spin readout of the nitrogen-vacancy center in diamond

David A. Hopper, Richard R. Grote, Annemarie L. Exarhos, and Lee C. Bassett

Phys. Rev. B **94**, 241201 — Published 9 December 2016

DOI: 10.1103/PhysRevB.94.241201

Near-Infrared-Assisted Charge Control and Spin Readout of the Nitrogen-Vacancy Center in Diamond

David A. Hopper,[1,2] Richard R. Grote,[1] Annemarie L. Exarhos,[1] and Lee C. Bassett[1,*]

[1] *Quantum Engineering Laboratory, Department of Electrical and Systems Engineering, University of Pennsylvania, Philadelphia, PA 19104 USA*

[2] *Department of Physics, University of Pennsylvania, Philadelphia, PA 19104 USA*

(Dated: November 22, 2016)

We utilize nonlinear absorption to design all-optical protocols that improve both charge state initialization and spin readout for the nitrogen-vacancy (NV) center in diamond. Non-monotonic variations in the equilibrium charge state as a function of visible and near-infrared optical power are attributed to competing multiphoton absorption processes. In certain regimes, multicolor illumination enhances the steady-state population of the NV's negative charge state above 90%. At higher NIR intensities, selective ionization of the singlet manifold facilitates a protocol for spin-to-charge conversion that dramatically enhances the spin readout fidelity. We demonstrate a 6-fold increase in the signal-to-noise ratio for single-shot spin measurements and demonstrate a pathway towards single-shot electron spin readout at room temperature.

The diamond nitrogen-vacancy (NV) center is a versatile solid-state qubit[1] and nanoscale sensor[2,3], exhibiting long spin coherence times at room temperature and all-optical mechanisms for qubit initialization and readout. Unfortunately, these convenient mechanisms are imperfect. The NV's intrinsic optical dynamics limit the charge and spin initialization purity well below unity[4–7] and only provide a low-fidelity spin-state readout[2,8,9]. These drawbacks impose substantial averaging requirements that diminish the full potential of the NV center as a qubit and quantum sensor[10].

Initialization and readout of NV spins are traditionally achieved through optical excitation and photoluminescence (PL) detection, respectively. Optical excitation, however, causes unavoidable cycling from the desired negative charge state (NV^-) into the neutral state (NV^0) with a different spin and orbital configuration. Charge-state transitions result from optical excitation of an electron from NV^- to the conduction band (ionization) and a hole from NV^0 to the valence band (recombination), which compete to produce a maximum steady-state NV^- population of $\sim 75\%$ using an optimized single excitation wavelength of 532 nm[7].

Traditional PL-based spin readout results from a spin-dependent inter-system crossing (ISC) between the triplet and singlet manifolds of NV^-[6,11,12]. In typical experiments, PL contrast only exists for the first $\sim$200 ns of excitation, during which time $\sim$0.01 PL photons are collected, on average. Therefore $\sim 10^4$ repeats are required to obtain adequate signal-to-noise ratio (SNR). This averaging requirement precludes important applications including projective[13] and partial[14] measurements of proximal nuclear spins, as well as verification of entanglement between remote NVs[15], all of which rely on a single-shot electron readout protocol that, at present, is only available at cryogenic temperatures[16].

Here, we demonstrate dramatic improvements in both charge initialization and spin readout fidelity by using multicolor illumination to manipulate the NV's orbital, spin, and charge-state dynamics. Our experiments uncover complex multiphoton absorption effects driven by visible and near-infrared excitation, resolving conflicting reports of both enhancement and quenching of NV^- PL under simultaneous illumination with 532 nm visible and 1064 nm light[17–20]. We use this knowledge to demonstrate a new protocol for efficient spin-to-charge conversion *via* selective ionization of the NV^- singlet that yields a 6-fold increase in the signal-to-noise ratio (SNR) for single-shot spin measurements and a pathway towards single-shot electron spin readout at room temperature.

Recent attempts to overcome the charge initialization problem include electrical gating[21] and doping[22], but the former yields deterministic initialization only in NV^0 and

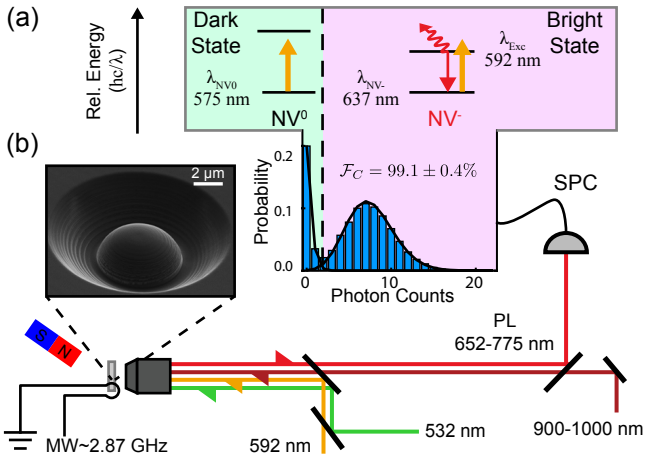

FIG. 1. Deterministic charge state readout of the NV center. (a) Illumination at 592 nm selectively excites the NV^- charge state (ZPL at 637 nm) and not NV^0 (ZPL at 575 nm). A typical photon distribution for a 3 ms readout duration is inset below (5000 cycles). (b) Diagram of the confocal microscope and electron micrograph of the solid immersion lens milled by a focused ion beam from the diamond surface. (ZPL: Zero-phonon line, MW: Microwave, SPC: Single Photon Counter).

the latter, while effective in stabilizing NV^-, also introduces impurities that reduce the spin coherence time. Several schemes have been proposed to address the readout problem. Protocols using quantum logic with nuclear spin ancillae[9,23] have achieved a 7-fold improvement in SNR over traditional PL measurements[2], at the expense of demanding technical and material requirements. An alternative approach was explored by Shields *et al.*[24], who demonstrated spin-to-charge conversion (SCC) through spin-dependent ionization of the NV^- triplet manifold using a visible pulse of light. Together with high-fidelity readout of the NV charge state[4] and extremely high photon collection efficiency, SCC yielded a 4-fold improvement in the single-shot SNR and reduced the spin readout noise to ∼3× the standard quantum limit (SQL). Nonetheless, a room-temperature protocol for single-shot electron-spin readout with SNR>1 is still lacking.

Figure 1 illustrates the experimental setup and the concept of high-fidelity charge readout. The technique exploits the blue-shifted absorption spectrum of NV^0 compared to NV^-, allowing for charge-dependent PL during 592 nm excitation. Precise tuning of the illumination power (∼100 nW) and readout time produces a strong PL contrast (SNR≈3) that allows for single-shot discrimination of the two charge states by introducing a photon-detection threshold condition (dashed black line in Fig. 1a). For low illumination power, the single-shot charge measurement is also non-destructive, which facilitates deterministic monitoring of the charge dynamics and the direct measurement of ionization and recombination rates from individual charge-transition events[7]. The photon-detection histogram shown in the inset of Fig. 1a corresponds to a single-shot fidelity $\mathcal{F}_c = 99.1 \pm 0.4\%$ and a non-destructivity exceeding 96%[25].

Individual NVs are addressed using a home-built scanning confocal microscope with three excitation sources (Fig. 1b). Continuous-wave 532 nm and 592 nm lasers are gated with acousto-optic modulators, and a 900-1000 nm band-pass-filtered supercontinuum source (hereafter termed NIR) produces picosecond pulses with a 40 MHz repetition rate that can be gated in time. A 6-µm-diameter solid immersion lens is fabricated around a preselected NV to increase the collection and excitation efficiency using an *in-situ* alignment technique and focused-ion-beam milling. Collected PL is filtered to select for NV^- in the 650-775 nm band and detected with a single-photon avalanche diode. In this configuration, we record ∼0.04 PL photons per 200 ns shot[25]. A ∼20 G magnetic field applied along the NV's symmetry axis splits the NV^- ground-state $m_s = \pm 1$ spin sublevels, and a 20 µm-diameter gold wire placed across the surface of the diamond is driven by pulsed microwaves to control the ground-state spin.

Figure 2 presents measurements of the steady-state PL and corresponding charge distribution under coincident excitation with 532 nm and NIR light. Both sets of measurements exhibit non-monotonic variations as a function of NIR power, P_{NIR}, connecting conflicting observations of PL quenching and enhancement in different regimes[17,18,20]. The direct correlation between the relative changes in PL (Fig. 2a) and the underlying charge distributions probed using single-shot readout (Fig. 2b) confirm the hypothesized role of charge-state modulation in these effects. Overall, the non-monotonic response and dependence on green power (P_{532}) hint at multiple processes that depend on the relative visible and NIR intensities. Below, we explore the role of NIR light in modulating the NV's charge dynamics in these different regimes.

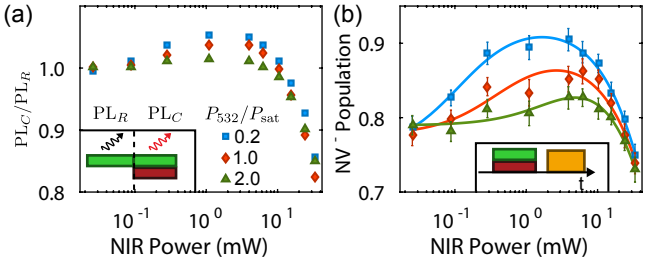

FIG. 2. Multicolor modulation of steady-state PL and charge. (a) PL due to coincident excitation at 532 nm and 900-1000 nm (PL_C), normalized by the reference PL level under 532 nm excitation alone (PL_R). The NIR excitation is modulated with a square wave at 5 kHz (inset). Experimental uncertainties are smaller than the symbols. (b) Steady-state population of NV^- (points) for the corresponding power combinations in (a), fit using a model described in the text (curves).

Notably, the PL enhancement observed with modest green and NIR powers in Fig. 2a is accompanied by an increase in the steady-state NV^- population (p_{minus}) to a maximum value of 91±0.6%, corresponding to an 18% improvement over the observed population under 532 nm illumination of 77%. This is, to our knowledge, the highest-purity all-optical initialization of NV^- yet reported. Furthermore, we anticipate that the spin purity should be maintained under this protocol since the spin-polarization rate exceeds the charge-switching rate in this regime by over two orders of magnitude[25,26].

Figure 3a uses a linear horizontal scale to present the same data as Fig. 2b (lowest green power) together with an analogous measurement combining 592 nm and NIR excitation. We observe an initial enhancement followed by suppression of p_{minus} in both cases, which implies this behavior is independent of the vastly different initial conditions produced by 532 nm and 592 nm light alone[7]. In contrast, the charge distributions observed in a similar experiment using only NIR light (red triangles in Fig. 3a) exhibit completely different dynamics, underscoring the crucial role of coupled, nonlinear optical processes.

To elucidate the underlying mechanisms, we use high-fidelity, non-destructive charge-state readout to directly measure the NV's ionization and recombination rates. After non-destructively determining the charge state, we apply an optical pulse with duration and intensity cho-

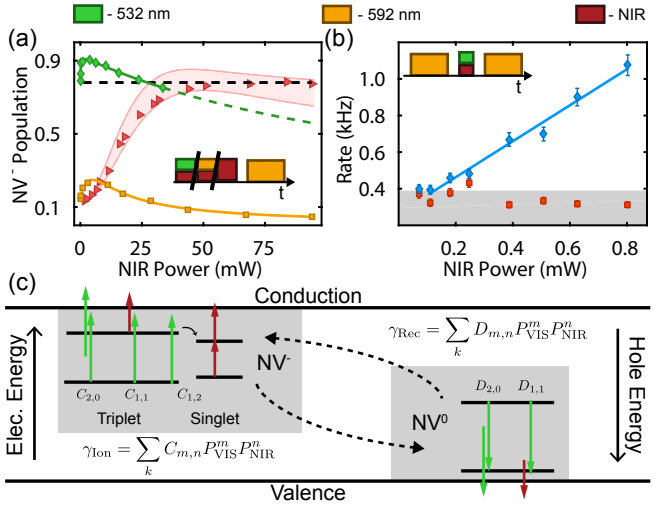

FIG. 3. Charge dynamics driven by multiphoton absorption. (a) NV^- population versus P_{NIR}, for fixed visible excitation at 532 nm (9 µW≃0.2P_{sat}, ♦), 592 nm (20 µW≃ 0.1P_{sat}, ▪), and for NIR light only (▸). Curves are fits described in the text. The shaded region indicates the 95% confidence interval for a simulation of the NIR data using separately measured rates[25]. (b) Recombination (♦) and ionization (▪) rates versus P_{NIR} for $P_{532} = 5.4\,\mu W \simeq 0.13 P_{sat}$. The shaded region indicates the noise floor. (c) NV energy diagram indicating allowed optical transitions and corresponding coefficients in the rate model. Insets in (a-b) depict the experimental pulse sequences for each measurement. Except where indicated by error bars, symbol sizes exceed the experimental uncertainty.

sen to induce ≪1 charge transition, and then measure the resulting state. Following many such measurements, the rates are calculated from the corresponding transition probabilities divided by the illumination duration.

Figure 3b shows the ionization and recombination rates as a function of P_{NIR} in the regime of NV^- enhancement (P_{532} is slightly lower than in Fig. 3a to reduce the charge-switching rates due to green light alone, but the steady-state maximum $p_{minus} = 91\%$ is unchanged). As expected, the rate for recombination is much larger than for ionization; in fact, the ionization rate is below the noise floor imposed by the 4% destructivity of the charge verification step.

The recombination rate's linear dependence on P_{NIR} implies that the mechanism driving NV^- enhancement involves a single NIR photon. The most likely candidate is a sequential absorption process in which a 532 nm photon promotes a hole to the excited state of NV^0, followed by the absorption of single NIR photon to promote the hole into the valence band, thus converting the center to NV^-. Based on the location of the NV's levels within the bandgap[7], an analogous ionization process is also allowed, but it is apparently ∼7 times less likely to occur[25]. This asymmetry could result from a combination of the ∼50% longer optical lifetime of NV^0[27] and different cross sections for NIR absorption by the NV^- and NV^0 excited states. We have also measured the ionization and recombination rates in the presence of NIR light alone[25]. They scale with P_{NIR}^3 and P_{NIR}^2, respectively, but are several orders of magnitude smaller than the corresponding rates in the presence of visible light.

To capture the effects of these competing nonlinear processes, we employ a master-equation model for the charge-state dynamics, schematically depicted in Fig. 3c. It includes the allowed orbital and charge transitions considering six levels that comprise the NV^- triplet and singlet manifolds, and the NV^0 ground and excited states. Each ionization or recombination process is assigned a coefficient, $C_{m,n}$ or $D_{m,n}$, respectively, where m and n are the respective number of visible and NIR photons required for that process. For example, the ionization rate for the process corresponding to $C_{m,n}$ is given by $C_{m,n} P_{VIS}^m P_{NIR}^n$. The total ionization or recombination rate is the sum of all the individual rates.

We apply this model to fit the steady-state charge distributions in Fig. 3a, using four parameters that quantify the relative weights between the ionization/recombination coefficients[25]. Differences between the experiments using 532 nm and 592 nm light are naturally explained by large differences in the cross section for NV^0 excitation that affect $D_{1,1}$ and $D_{2,0}$. The charge distributions observed under NIR-only illumination in Fig. 3a do not, in fact, represent the steady-state population, due to the relative weakness of NIR-only nonlinear absorption. Nonetheless, we can quantitatively reproduce those data by adapting our model to account for the slow underlying rates(<kHz) and a partially destructive charge-state readout[25].

Whereas the NV^- enhancement observed at low powers in Fig. 3a is driven by the asymmetry in $D_{1,1}/C_{1,1}$, the suppression at increasing powers results from the higher-order term $C_{1,2}$. This process corresponds to ionization of NV^- *via* absorption of one visible and two NIR photons. A candidate mechanism is NIR-induced ionization from the metastable singlet ground state. The singlet manifold is populated through the ISC by visible excitation, and exhibits a zero phonon line at 1042 nm accompanied by a broad phonon-assisted-absorption sideband overlapping our NIR excitation source[28,29].

To confirm the singlet's role in quenching NV^- at high P_{NIR}, we use the generalized measurement sequence depicted in Fig. 4a to probe the time-domain ionization dynamics. Since we are interested in NV^- as a starting state, we use a non-destructive charge-verification step to provide a high-purity, post-selected $p_{minus} = 96.8 \pm 0.4\%$. The effects of an arbitrary sequence of visible, NIR, and microwave pulses on the NV's charge are then measured using a high-fidelity readout step. In Fig. 4b, we initialize the ground-state spin in either the $m_s = -1$ or $m_s = 0$ sublevel before applying a varying-duration 532 nm shelving pulse followed by a 400 ns, 95 mW train of NIR pulses. The resulting spin-dependent contrast in the final NV^- population is the hallmark of SCC, and the preferential ionization of $m_s = -1$ over $m_s = 0$ suggests that the singlet population is being ionized. To confirm this hy-

pothesis, we fix the shelving pulse duration at τ_s =200 ns to produce a maximum charge contrast, initialize into $m_s = -1$, and vary the delay, τ_d, to the 400 ns NIR pulse train (Fig. 4c). The resulting p_{minus} exhibits exponential decay with a timescale commensurate with the metastable singlet's lifetime ($\tau_{\mathrm{Fit}} = 182 \pm 10$ ns)[16,28].

The transient population of the NV$^-$ singlet manifold is highly spin dependent. Therefore, singlet-selective ionization provides a promising means for SCC. The maximum SCC contrast observed in Fig. 4(b) ($\sim$ 7% for τ_s = 200 ns) is limited in our current setup by the available NIR pulse energy (2 nJ), which ionizes the singlet with per-pulse probability $\sim$6%. The full NIR pulse train ionizes the singlet with 32% probability[25]. Despite this incomplete ionization, we can enhance the SCC efficiency substantially by repeating the shelve-ionize pulse sequence N times (Fig. 4d). Crucial to this multi-SCC method is the choice of a shelving pulse that excites the triplet manifold once on average, which we found to occur when $\tau_s = 30$ ns with a power near saturation. The spin contrast increases rapidly with N to $\sim$ 25% and eventually saturates due to a combination of effects including incomplete ionization, accidental ionization of the triplet, the small ISC probability for $m_s = 0$, and imperfect spin initialization. Fits to the data in Fig. 4d reflect an extended six-level master-equation model that accounts for all these factors[25].

To quantify the performance of multi-SCC spin readout, we consider the single-shot SNR corresponding to a measurement of the spin contrast, i.e., the difference between a spin prepared in $m_s = 0$ and ± 1 (Fig. 4e). The noise includes contributions from both imperfect SCC efficiency and shot noise in the charge-state readout[25]. Our demonstrated protocol exhibits a single-shot SNR = 0.32, corresponding to a spin-readout noise 4.6$\times$ the SQL and constituting a 6-fold improvement over traditional PL readout, even for our SIL-enhanced device[25]. Given NIR pulses that ionize the singlet with 100% probability, we predict a further $\sim$2.6-fold improvement to SNR = 0.83, corresponding to a single-shot readout fidelity exceeding 75% and spin-projection noise 1.9$\times$ the SQL. The singlet-selective ionization can be optimized by adjusting the wavelength, pulse width, and repetition rate of the NIR pulse train to compensate the singlet's small optical cross section and short excited-state lifetime ($\sim$1 ns)[28], and with the use of cavities to boost the optical interaction. These values all include the detrimental effect of imperfect spin initialization (we infer $\sim$85% spin purity). With improved spin purity, multi-SCC should approach a maximum SNR$\sim$1.9, limited by the intrinsic $\sim$10:1 spin-dependent ISC branching ratio[30]. This ideal case corresponds to an upper bound of the single-shot spin readout fidelity of 90%.

In conclusion, we use previously unexplored multi-photon absorption mechanisms to improve both initialization and readout of diamond NV spins. Deliberate tuning of coincident 532 nm and NIR intensities boosts the steady-state NV$^-$ population to 91.0 $\pm$ 0.6%. Carefully timed optical pulse sequences generate efficient spin-to-charge conversion and a universal spin-readout enhancement over the standard approach. Crucially, these all-optical techniques are applicable to both single-NV and ensemble experiments where high-contrast charge measurements have recently been demonstrated[31,32]. Furthermore, these enhancements can lead to significant advances for many research avenues including magnetometry[2] and operations involving nuclear spins[33,34], where signal averaging is a critical bottleneck. Future experiments exploring the SCC dynamics and performance in ensembles as well as nanodiamonds will further motivate the adoption of these enhanced spin readout techniques for diverse applications. Ultimately, as the SCC efficiency approaches the ideal limit of single-shot electron spin readout, it will enable room-temperature applications of protocols that were previously relegated to cryogenic (<10 K) temperatures, including projective and partial measurements of nuclear spins[13,14] and verification of multi-spin entanglement[15].

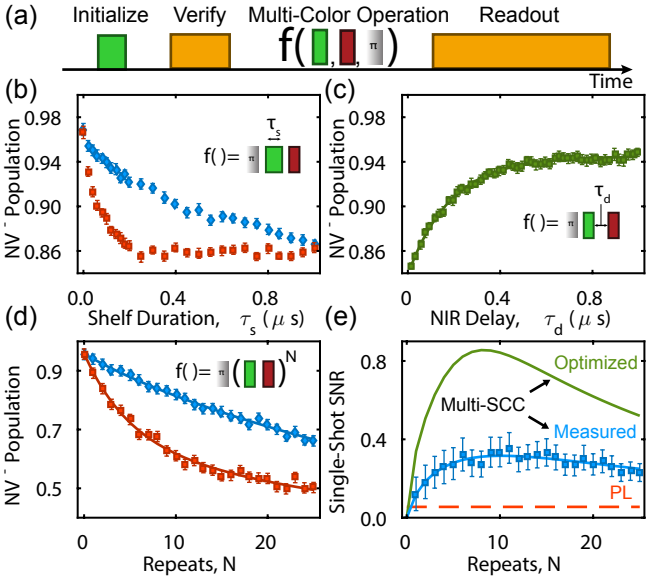

FIG. 4. Spin-to-charge conversion *via* singlet ionization. (a) Generalized pulse diagram for probing time-domain charge dynamics. (b) Resulting charge state as a function of 532 nm shelf duration followed by a 400 ns NIR pulse for spins prepared in $m_s = 0$ (♦) and $m_s = -1$ (▪). (c) Resulting charge state as a function of the delay between a 200 ns, 532 nm shelving pulse and a 400 ns NIR pulse, for a spin prepared in $m_s = -1$. (d) Final charge state as a function of SCC repeats for different initial spin states prepared as in (b). (e) Spin-readout SNR comparison of traditional PL (red), measured multi-SCC (blue), and the optimized multi-SCC protocol assuming 100% singlet ionization (green).

ACKNOWLEDGMENTS

This work was supported by the University of Pennsylvania and a National Science Foundation CAREER grant (EECS-1553511). The authors thank Kameron Oser for helpful discussions.

* Corresponding author.
Email address: lbassett@seas.upenn.edu

[1] D. D. Awschalom, L. C. Bassett, A. S. Dzurak, E. L. Hu, and J. R. Petta, Science **339**, 1174 (2013).

[2] I. Lovchinsky, A. O. Sushkov, E. Urbach, N. P. de Leon, S. Choi, K. De Greve, R. Evans, R. Gertner, E. Bersin, C. Müller, L. McGuinness, F. Jelezko, R. L. Walsworth, H. Park, and M. D. Lukin, Science **351**, 836 (2016).

[3] S. Karaveli, O. Gaathon, A. Wolcott, R. Sakakibara, O. A. Shemesh, D. S. Peterka, E. S. Boyden, J. S. Owen, R. Yuste, and D. Englund, Proc. Natl. Acad. Sci. USA **113**, 3938 (2016).

[4] G. Waldherr, P. Neumann, S. F. Huelga, F. Jelezko, and J. Wrachtrup, Phys. Rev. Lett. **107**, 090401 (2011).

[5] G. Waldherr, J. Beck, M. Steiner, P. Neumann, A. Gali, T. Frauenheim, F. Jelezko, and J. Wrachtrup, Phys. Rev. Lett. **106**, 157601 (2011).

[6] L. Robledo, H. Bernien, T. van der Sar, and R. Hanson, New J. Phys. **13**, 025013 (2011).

[7] N. Aslam, G. Waldherr, P. Neumann, F. Jelezko, and J. Wrachtrup, New J. Phys. **15**, 013064 (2013).

[8] J. M. Taylor, P. Cappellaro, L. Childress, L. Jiang, D. Budker, P. R. Hemmer, A. Yacoby, R. Walsworth, and M. D. Lukin, Nature Phys. **4**, 810 (2008).

[9] L. Jiang, J. S. Hodges, J. R. Maze, P. Maurer, J. M. Taylor, D. G. Cory, P. R. Hemmer, R. L. Walsworth, A. Yacoby, A. S. Zibrov, and M. D. Lukin, Science **326**, 267 (2009).

[10] D. P. DiVincenzo, Fortschritte der Physik **48**, 771 (2000).

[11] E. van Oort, N. B. Manson, and M. Glasbeek, J. Phys. C: Solid State Phys. **21**, 4385 (1988).

[12] M. W. Doherty, N. B. Manson, P. Delaney, F. Jelezko, J. Wrachtrup, and L. C. Hollenberg, Phys. Rep. **528**, 1 (2013).

[13] W. Pfaff, T. H. Taminiau, L. Robledo, H. Bernien, M. Markham, D. J. Twitchen, and R. Hanson, Nature Phys. **9**, 29 (2013).

[14] M. S. Blok, C. Bonato, M. L. Markham, D. J. Twitchen, V. V. Dobrovitski, and R. Hanson, Nature Phys. **10**, 189 (2014).

[15] H. Bernien, B. Hensen, W. Pfaff, G. Koolstra, M. S. Blok, L. Robledo, T. H. Taminiau, M. Markham, D. J. Twitchen, L. Childress, and R. Hanson, Nature **497**, 86 (2013).

[16] L. Robledo, L. Childress, H. Bernien, B. Hensen, P. F. A. Alkemade, and R. Hanson, Nature **477**, 574 (2011).

[17] M. Geiselmann, R. Marty, F. J. Garcia de Abajo, and R. Quidant, Nature Phys. **9**, 785 (2013).

[18] L. P. Neukirch, J. Gieseler, R. Quidant, L. Novotny, and A. N. Vamivakas, Opt. Lett. **38**, 2976 (2013).

[19] N. D. Lai, O. Faklaris, D. Zheng, V. Jacques, H.-C. Chang, J.-F. Roch, and F. Treussart, New Journal of Physics **15**, 033030 (2013).

[20] P. Ji and M. V. G. Dutt, Phys. Rev. B **94**, 024101 (2016).

[21] Y. Doi, T. Makino, H. Kato, D. Takeuchi, M. Ogura, H. Okushi, H. Morishita, T. Tashima, S. Miwa, S. Yamasaki, P. Neumann, J. Wrachtrup, Y. Suzuki, and N. Mizuochi, Phys. Rev. X **4**, 011057 (2014).

[22] Y. Doi, T. Fukui, H. Kato, T. Makino, S. Yamasaki, T. Tashima, H. Morishita, S. Miwa, F. Jelezko, Y. Suzuki, and N. Mizuochi, Phys. Rev. B **93**, 081203 (2016).

[23] M. Steiner, P. Neumann, J. Beck, F. Jelezko, and J. Wrachtrup, Phys. Rev. B **81**, 035205 (2010).

[24] B. J. Shields, Q. P. Unterreithmeier, N. P. de Leon, H. Park, and M. D. Lukin, Phys. Rev. Lett. **114**, 136402 (2015).

[25] See the supplemental information online for further details.

[26] X.-D. Chen, L.-M. Zhou, C.-L. Zou, C.-C. Li, Y. Dong, F.-W. Sun, and G.-C. Guo, Phys. Rev. B **92**, 104301 (2015).

[27] G. Liaugaudas, G. Davies, K. Suhling, R. U. A. Khan, and D. J. F. Evans, J.Phys.: Condens. Matter **24**, 435503 (2012).

[28] V. M. Acosta, A. Jarmola, E. Bauch, and D. Budker, Phys. Rev. B **82**, 201202 (2010).

[29] P. Kehayias, M. W. Doherty, D. English, R. Fischer, A. Jarmola, K. Jensen, N. Leefer, P. Hemmer, N. B. Manson, and D. Budker, Phys. Rev. B **88**, 165202 (2013).

[30] M. L. Goldman, M. W. Doherty, A. Sipahigil, N. Y. Yao, S. D. Bennett, N. B. Manson, A. Kubanek, and M. D. Lukin, Phys. Rev. B **91**, 165201 (2015).

[31] H. Jayakumar, J. Henshaw, S. Dhomkar, D. Pagliero, A. Laraoui, N. B. Manson, R. Albu, M. W. Doherty, and C. A. Meriles, Nat. Commun. **7**, 12660 (2016).

[32] S. Dhomkar, J. Henshaw, H. Jayakumar, and C. Meriles, Science Advances **2**, e1600911 (2016).

[33] T. H. Taminiau, J. J. T. Wagenaar, T. van der Sar, F. Jelezko, V. V. Dobrovitski, and R. Hanson, Phys. Rev. Lett. **109**, 137602 (2012).

[34] S. Kolkowitz, Q. P. Unterreithmeier, S. D. Bennett, and M. D. Lukin, Phys. Rev. Lett. **109**, 137601 (2012).